The Binding of W7, an Inhibitor of Striated Muscle Contraction, to Cardiac Troponin C†

Ryan M. B. Hoffman, Monica X. Li, and Brian D. Sykes*

CIHR Group in Protein Structure and Function, Department of Biochemistry, University of Alberta, Edmonton, Alberta, Canada T6G 2H7

Received August 9, 2005; Revised Manuscript Received October 11, 2005

ABSTRACT: W7 is a well-characterized calmodulin antagonist. It decreases the maximal tension and rate of ATP hydrolysis in cardiac muscle fibers. Cardiac troponin C (cTnC) has been previously implicated as the mechanistically significant target for W7 in the myofilament. Two-dimensional NMR spectra ({^{1}H,^{15}N}- and {^{1}H,^{13}C}-HSQCs) were used to monitor the Ca^{2+}-dependent binding of W7 to cTnC. Titration of cTnC·3Ca^{2+} with W7 indicated binding to both domains of the protein. We examined the binding of W7 to the separated domains of cTnC to simplify the spectral analysis. In the titration of the C-terminal domain (cCTnC·2Ca^{2+}), the spectral peaks originating from a subset of residues changed nonuniformly, and could not be well-described as single-site binding. A global fit of the cCTnC·2Ca^{2+} titration data to a two-site, sequential binding model (47 residues simultaneously fit) yielded a dissociation constant (Kd1) of 0.85−0.91 mM for the singly bound state, with the second dissociation constant fit to 3.40−3.65 mM (≥4 × Kd1). The titration data for the N-terminal domain (cNTnC·Ca^{2+}) was globally fit to single-site binding model with a Kd of 0.15−0.30 mM (41 residues fit). The data are consistent with W7 binding to each domain's major hydrophobic pocket, coordinating side chains responsible for liganding cTnI. When in muscle fibers, W7 may compete with cTnI for target sites on cTnC.

Cardiac muscle contracts upon the release of Ca^{2+} from the sarcoplasmic reticulum. Cardiac troponin C (cTnC[1]) acts as a Ca^{2+} sensor: Ca^{2+}-binding to the N-terminal domain of cTnC (cNTnC) initiates the conformational transitions which culminate in the contraction of the myofilament (reviewed in refs *1, 2*). The conformational transitions in cNTnC are transmitted to the myofilament through direct interactions with cardiac troponin I (cTnI). Perturbations to these essential protein−protein interactions are central to cardiac dysfunction in both causative (as in familial cardiac hypertrophy) and secondary (as in congestive heart failure) aspects (*3*). There is much ongoing effort directed toward the detection and correction of cardiac contractile dysfunction. Chemotherapeutic interventions are currently in use and under development.

Cardiotonic drugs, such as levosimendan, are clinically useful when forestalling heart failure (*3, 4*). These agents increase the contractile force of the heart. Levosimendan's cardiotonic mechanism is thought to feature direct sensitization of cTnC to Ca^{2+} (*5*). Such a drug mechanism is therapeutically desirable because intracellular [Ca^{2+}] is not perturbed, preserving the regulation of other Ca-based signaling pathways (*4, 5*). Toward defining generalized cardiotonic structure−activity relationships, several cTnC·ligand complexes have been solved to high precision. The structures of cNTnC·Ca^{2+}·bepridil·$cTnI_{147-163}$ (*6*) and cCTnC·2Ca^{2+}·EMD57033 (*7*) both visualize similar protein−drug interactions, albeit in different domains of cTnC. Bepridil and EMD57033 both bind to a homologous hydrophobic pocket nestled between two EF hands. The generality of this binding site is further implicated by the recent X-ray structure of the Ca^{2+}-activated skeletal troponin complex (*8*). In that study, the polyoxyethylene detergent Anapoe binds to the N-domain of TnC, in an analogous location to bepridil in cNTnC·Ca^{2+}bepridil·$cTnI_{147-163}$. Anapoe is reported to be essential for the production of sufficiently ordered troponin crystals to allow for diffraction to high resolutions. The authors surmise that ligand binding stabilizes unique microstates of cTnC's native ensemble, and report that Anapoe enhances the contractility of skinned, permeabilized muscle fibers (*8*).

The drug binding sites in cTnC have subtle structure−activity relationships. Both computational (*9*) and experimental (*10, 11*) studies have concluded that multiple binding sites or modes could exist for several cTnC·ligand interactions. A study by Kleerekoper et al. suggested that there are two drug binding sites in cNTnC's hydrophobic pocket, with one site (demarked by Met 45, 60, and 80) conferring Ca^{2+}-sensitizing effects, and the other site (containing Met 47, 81, and 85) also being capable of coordinating ligand, but being capable of occluding $cTnI_{147-163}$ and therefore conferring Ca^{2+}-desensitizing effects (*10*). The high-resolution

† This work is supported by the Canadian Institutes of Health Research, and the Heart and Stroke Foundation of Canada.

* Corresponding author. E-mail: brian.sykes@ualberta.ca. Mailing address: Room 419, Medical Sciences Bldg., University of Alberta, Edmonton, Alberta, Canada T6G 2H7. Phone: (780) 492-5460. Fax: (780) 492-0886.

[1] Abbreviations: NMR, nuclear magnetic resonance; TnC, troponin C; cTnC, cardiac TnC; cNTnC, N-terminal domain of cTnC (residues 1−89); cCTnC, C-terminal domain of cTnC (residues 91−161); CaM, calmodulin; 2D, two-dimensional; Kd, dissociation constant; ppm, parts per million; Δδ, chemical shift perturbation.

10.1021/bi051583y CCC: $30.25
Published on Web 11/10/2005

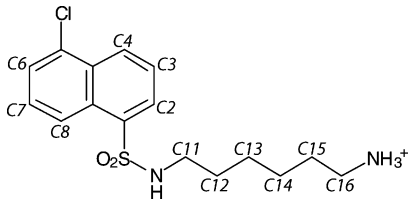

FIGURE 1: The chemical structure of W7 (*N*-[6-aminohexenyl]-5-chloro-naphthalenesulfonamide). Standard numbering for carbon atoms is shown in italics.

details of cNTnC·ligand interactions are therefore important to the biochemical activity of the ligand. Another pressure toward discriminating binding determinants is the prevalence of structural homologues with disparate and essential biochemical roles, including calmodulin (CaM) and skeletal TnC. Binding promiscuity largely obviates the clinical usefulness of therapeutic drugs. An understanding of binding promiscuity therefore empowers rational drug design.

W7 is a well-characterized CaM antagonist, widely used to dissect Ca^{2+}-mediated signaling pathways. Previous studies have reported that W7 binds CaM with a range of per-domain stoichiometries (*1*−*6*), and to sites of weak (Kd = 200 μM) and strong (11 μM) affinities (*12*). The binding of W7 to chicken TnC·4Ca^{2+} was also described with mixed binding modes, with the stronger Kd being 25 μM. This compound inhibits muscle contraction in skinned muscle fibers and in perfused hearts; cTnC has been implicated as the mechanistically relevant target for W7 in the myofilament (*13*). W7 and its analogues have two functional moieties: an aromatic "head" and an amine "tail" (Figure 1). Both moieties are required for activity. NMR spectroscopy has been employed toward the rationalization of W7's mechanism of action. A previously published structure of CaM·W7 visualized a single molecule of W7 binding to each domain (*14*). An NMR study on J8 (*15*), a closely related W7 analogue, reported multiple orientations of J8 within the binding pocket of CaM (multiple binding "poses"), with no definable conformation for the tail moiety. The study of the binding of W7 to cTnC, a protein sharing ~50% identity with CaM, would clarify the mechanistic picture as TnC and CaM have structurally analogous drug (and target peptide) binding sites (*16*).

Here we report the titration of W7 into Ca^{2+}-saturated samples of cCTnC or cNTnC, monitoring structural changes with 2D-NMR spectra. By inspection, the data are indicative of mixed binding modes. Binding equilibria are modeled using all titratable backbone amide signals thereby reconciling the site-specific NMR data with global binding constants.

METHODS

Sample Preparation. The cloning, mutagenesis, and expression of human cNTnC (C35S, C84S; residues 1−89) and cCTnC (residues 91−161) have been reported (*17*). ^{15}N- and {^{15}N,^{13}C}-labeled protein was expressed and purified as previously described [*18*, *7*, preps for cNTnC and cCTnC, respectively]. W7 (*N*-[6-aminohexenyl]-5-chloronaphthalenesulfonamide) was purchased from Sigma-Aldrich as a dihydrochloride salt. Stock solutions of W7 (all around 130 mM) in d_6-DMSO was prepared for titrations. The stock was stored at −20 °C, and was protected from exposure to light. W7 concentrations were determined gravimetrically and corrected with UV absorbance measurements (extinction coefficient from ref *19*). NMR samples were prepared through reconstitution of lyophilized protein into 100 mM KCl, 10 mM imidazole, 10% D_2O. Protease inhibitor cocktail I (Calbiochem, Lot B48045), DSS (0.17 mM), and NaN_3 (0.01%) were added; $CaCl_2$ was added to 10 mM. Samples were brought to pH 6.7 (uncorrected value) with NaOH (~30 μL of 1 M NaOH). Samples were filtered through a Millipore Spin-X column (0.22 μL pore size) and decanted into a 5 mm NMR tube. Sample volumes were 500 μL, containing 0.5−2 mM protein. Protein concentrations were determined by amino acid analysis. Titrations were initially performed with ^{15}N-labeled samples (one replica each for cNTnC and cCTnC) and were repeated with {^{15}N,^{13}C}-labeled samples.

NMR Spectroscopy. NMR data were acquired at 30 °C on a Unity Inova 500 MHz spectrometer possessing a triple resonance probe and Z-pulsed field gradient. The sample was not spun. The experiments were implemented in Biopack (Varian Inc.). All spectra were processed with NMRPipe/NMRDraw (*20*). Processing featured forward-back linear prediction in the indirect dimension, and mild apodization and zero filling prior to Fourier transformation (in both dimensions). Peak picking and analysis was performed with the NANUC distribution of NMRView (*21*) as maintained by Pascal Mercier (Chenomx Inc.).

Titrations. For both cNTnC and cCTnC, {^{1}H,^{15}N}-HSQC and {^{1}H,^{13}C}-HSQC spectra were acquired at incremental concentrations of W7. The titration of ^{15}N-labeled cNTnC had an initial protein concentration of 0.50 mM; $[W7]_{total}$ was 0, 0.069, 0.139, 0.208, 0.277, 0.414, 0.551, 0.688, 0.959, 1.495, and 2.542 mM (11 data points). This titration is the source of the 2D-{^{1}H,^{15}N}-HSQC data presented here. A second sample of cNTnC, with {^{15}N,^{13}C}-labeling, was also titrated; the initial protein concentration was 1.25 mM, and $[W7]_{total}$ was varied between 0, 0.120, 0.361, 0.833, 1.426, 2.361, 3.509, and 4.630 mM (8 data points). This sample is the source of the 2D-{^{1}H,^{13}C}-HSQC spectra presented here. A 2D-{^{1}H,^{15}N}-HSQC in the titration series for this sample suffered data corruption and was not analyzed. The titration of ^{15}N,^{13}C-labeled cCTnC had an initial protein concentration of 1.76 mM, and $[W7]_{total}$ was varied between 0, 0.107, 0.322, 0.960, 1.80, 2.62, 3.84, and 5.02 mM (8 points). The {^{1}H,^{15}N}- and {^{1}H,^{13}C}-HSQC data presented here are from the same trial.

Most steps in the analysis were performed with programs written in-house. Spectra were peak-picked and assigned at similar contour heights. Assignments were done semiautomatically using a script by Pascal Mercier. Peak coordinates were manually verified. Chemical shift changes were summed in both dimensions (with the Pythagorean theorem) and converted into Xcrvfit (*22*) input files using scripts written in Perl. The optional scaling of ^{15}N by $^{1}/_{5}$ was implemented at this point. The site-specific Kds varied considerably depending on which residue was considered. An algorithm was devised and implemented (in Mathematica) to fit curves to a maximal sampling of titration-perturbed residues. The input data (assigned NMRView peak lists), and the scripts used to process this data, are available from the authors. A typical least squares curve fitting protocol was automated so that it was applied to each assigned residue in a titration series of 2D-NMR spectra. Instead of fitting all parameters

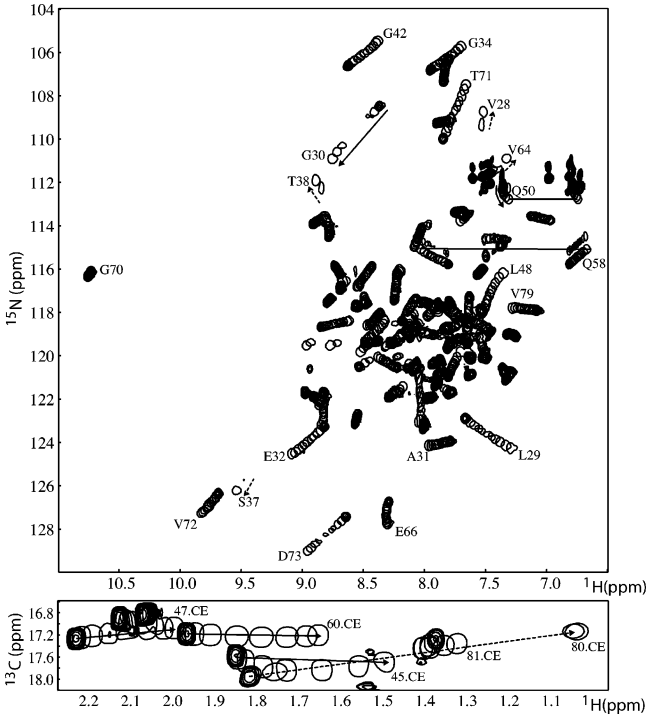

FIGURE 2: Titration of W7 into cNTnC·Ca^{2+}, monitored with {^{1}H,^{15}N}-HSQC (top) and {^{1}H,^{13}C}-HSQC (bottom) NMR spectra. The initial point of the titration is shown with filled contours. Intermediate and final points are displayed with open contours. The final increments are assigned. Arrows indicate the paths undergone by the cross-peaks; dashed lines indicate the most probable trajectory for extensively broadened peaks. Top: Most backbone amide signals shift linearly. Amide side chain cross-peaks from Q50 and Q58 are titratable (each side chain generates two cross-peaks, which are connected with lines). Some residues' cross-peaks broaden over the middle points of the titration. Bottom: All methionine Cϵ methyl cross-peaks are titratable. The cross-peaks from M80 and M81 shift in distinct ways.

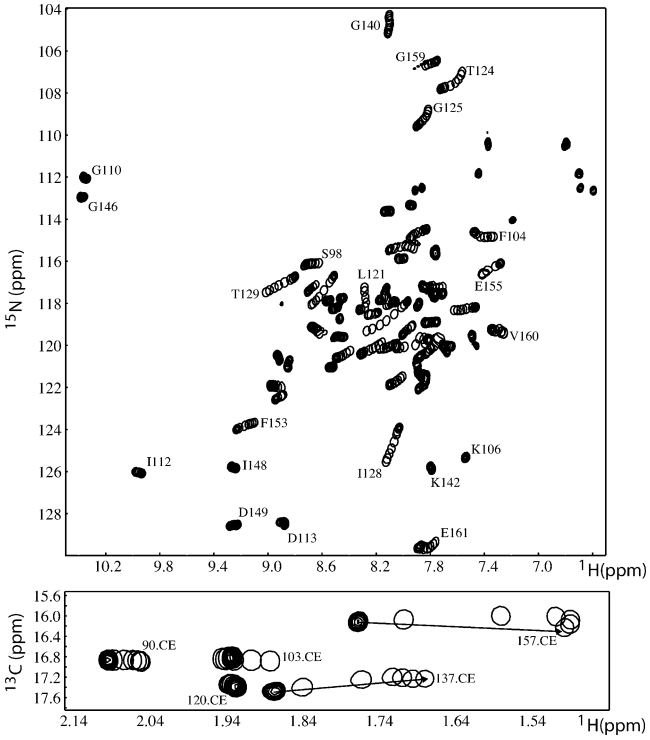

FIGURE 3: Titration of W7 into cCTnC·2Ca^{2+}. The depictions are as in Figure 2. Chemical shift changes are similar in magnitude to those observed for cNTnC·Ca^{2+}·W7. Unlike the titration of cNTnC·Ca^{2+} with W7, many residues' {^{1}H,^{15}N} cross-peaks move in curved paths over the titration. This is indicative of multiple binding modes. No line broadening is readily apparent.

to a given cross-peak's titration curve, however, the dissociation constant(s) were fixed at a "guess value" for the entire set of titration curves. A global error function—the sum of root-mean-square errors for all local fits—was then minimized, while manually varying the global Kds, as a grid search. Initially the fitting routine used a numerical cutoff to exclude extremely poor local fits from the global fit, tolerating local RMSEs <10. Errors this high were observed because some residues' titration series were only partially correctly assigned (for example, due to spectral overlap), but were included in the automated analysis up until this point, or because the residues were not significantly titratable. Once the extremely spurious fits were eliminated from the analysis (culling them from the input), the list of conserved residues was fixed. After this point, local fits were never excluded from global fits. The grid search was then repeated over more finely spaced query Kds. In this way, Kds were obtained that demonstrated maximal agreement with the entire data set.

RESULTS

Titration of W7 into cTnC. W7 was titrated into NMR samples of full-length cTnC, and chemical shift changes were monitored with 2D-{^{1}H,^{15}N}-HSQC or 2D-{^{1}H,^{13}C}-HSQC NMR spectra. Such NMR spectra correlate amide ^{15}N or aliphatic ^{13}C nuclei with covalently bonded ^{1}H. These NMR experiments monitor, at atomic resolution, changes in the chemical environment, and therefore reflect structural changes in a protein due to the binding of a ligand. The NMR cross-peaks could be tracked from their previously assigned (*23*) starting coordinates (chemical shifts), through each increment of the titration, to their final positions. The majority of the backbone 2D-{^{1}H,^{15}N}-HSQC cross-peaks changed their coordinates in the spectra as W7 was titrated into intact cTnC. The changes in chemical shift were broadly distributed across cTnC's primary structure, indicating binding of W7 to each domain of cTnC. To simplify the analysis, the titration was repeated using the separated N- and C-terminal domains of cTnC. These results are presented here; the analysis of intact cTnC will be presented elsewhere.

The titration of W7 into cNTnC·Ca^{2+}, as monitored with 2D-HSQC NMR spectra, is shown in Figure 2. Most 2D-{^{1}H,^{15}N}-HSQC cross-peaks (Figure 2, top) shift "linearly", meaning the initial, intermediate, and final chemical shifts for a given NMR cross-peak can be connected with a straight line. Exceptions to this pattern include cross-peaks that do not shift, or that deviate from linearity. Figure 2, top, shows two titratable backbone amide cross-peaks that shift along linear paths until the final increments. One of these, belonging to L48, is located in the linker region connecting cNTnC's first (non-Ca^{2+}-coordinating) EF hand with the second EF hand. The other, corresponding to E66, is localized to the Ca^{2+}-binding site. Many of the amide cross-peaks undergo changes in line shape over the titration: L29, G30, and D73 are noteworthy examples. This line broadening indicates exchange kinetics on the intermediate NMR time scale at these specific sites (see Discussion). V28, S37, T38, and V64 are extensively broadened to the point of being

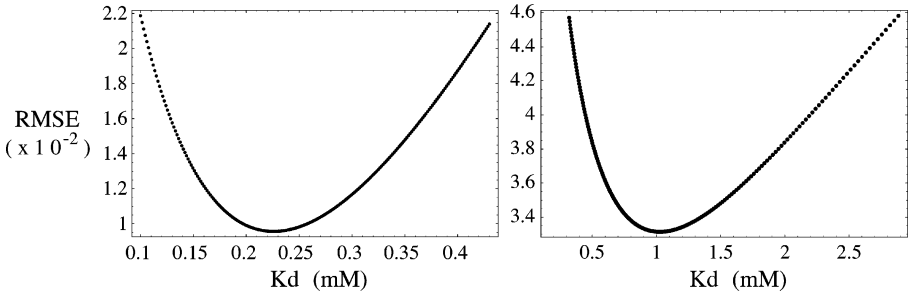

FIGURE 4: Left: Determination of a global Kd for the cNTnC·Ca^{2+}·W7 complex within a single-site binding model. The vertical axis shows the sum of RMSEs for the single-site fits, given a particular Kd (horizontal axis). The global minimum RMSE occurs over the interval of 0.15−0.30 mM. Over this range, 41 {^{1}H,^{15}N}-HSQC signals contribute to the fit. The algorithm used to obtain global fits automatically culls fits with RMSEs over 100. Right: Determination of a global, single-site Kd for cCTnC·2Ca^{2+}·W7. The Kd obtained is in the interval of 0.50−1.50 mM, with 52 amide signals contributing to the fit.

unobservable near the midpoints of the titration. These signals shift in directions consistent with the "opening" of cNTnC, usually effected through the binding of $cTnI_{147-163}$ to cNTnC·Ca^{2+} (*24*).

Nuclei located in Gln and Met side chains recapitulate the chemical shift changes reported by backbone amide nuclei. The amide side chain cross-peaks of Q50 and Q58 are titratable (Figure 2, top). 2D-{^{1}H,^{13}C}-HSQC cross-peaks originating from Met Cϵ methyl groups (Figure 2, bottom) show extensive changes over the titration. Cross-peaks from M47, M60, and M80 shift linearly as W7 is added to the sample. M80 experiences notable exchange broadening, with the cross-peaks in the midpoint of the titration being broadened to the point of being unobservable. M81 and M45's cross-peaks shift nonlinearly; M81's path is so nonlinear as to have a sharply defined inflection point at the midpoint of the titration. The close proximity of M80 and M81 in the primary structure is not reflected in their Cϵ methyl groups' spectral behavior over the titration.

Figure 3 shows cCTnC's 2D-{^{1}H,^{15}N}-HSQC and 2D-{^{1}H,^{13}C}-HSQC spectra at incremental concentrations of W7. Chemical shift changes due to W7 binding are extensive in magnitude and in their distribution over the primary structure, as observed for cNTnC. No changes in line shape are observed over the titration. A subset of {^{1}H,^{15}N} cross-peaks shift nonlinearly, including F104, L121, T124, G125, and E161 (Figure 3, top). Most of these residues are located in the linker region between the EF and GH subdomains. The nonlinearity is pronounced and evident near the midpoint of the titration. The amide side chain cross-peaks do not shift over the titration. The Met Cϵ methyl spectral changes (Figure 3, top) are similar to those seen for cNTnC, but most of the cross-peaks shift in a nonlinear fashion. The paths of M157 and M103's methyl cross-peaks reveal sharply defined inflection points, as for M81 in cCTnC.

Analysis of Binding Equilibria. The coordinates of each assigned 2D-{^{1}H,^{15}N} cross-peak, at each increment of the titration series, were extracted into tables (see Methods). Initially, only {^{1}H,^{15}N} signals shifting $\geq$0.15 ppm were considered, and the titration curves were examined individually. The data were fitted to a single-site binding model to obtain dissociation constants (Kds) (*25*). Examination of the individually fitted titration curves revealed a large variation in the Kds between differing amide sites. We sought to minimize the impact of fitting error through fitting all of the titration curves to the same Kd (see Methods). Figure 4 shows the global root-mean-square error (RMSE) as a function of Kd, for a single site binding model (P + L $\rightleftharpoons$ P·L), and for the titrations of cNTnC·Ca^{2+} and cCTnC·2Ca^{2+}. This analysis reveals the range of Kd values over which the RMSE is minimal. This analysis was applied to the titration data of both cNTnC·Ca^{2+} (Figure 4, left) and cCTnC·2Ca^{2+} (Figure 4, right); the global binding constants thus obtained are 0.15−0.30 mM and 0.50−1.50 mM, respectively. The site-specific fits for the cNTnC·W7 titration, consistent with the global Kd, are shown in Figure 5.

The analysis of the {^{1}H,^{15}N}-monitored cCTnC·2Ca^{2+}·W7 titration identified a number of signals that were poorly described by a single site binding model. Such signals shift extensively (>1 ppm) over the titration, making the observed shifts much larger than the uncertainty in peak coordinates. Therefore, these titration signals have sufficient precision to justify the consideration of more elaborate binding models. A two-site, sequential binding model (P + L $\rightleftharpoons$ P·L $\rightleftharpoons$ P·L_2) (*25*) allowed for an accurate fit to these data. A global fit to this binding model was also attempted. The global Kd1 and Kd2 were determined in a fashion similar to the analysis with the single-site binding model, but a two-dimensional grid search was necessitated. Figure 7 shows the values of Kd1 and Kd2 producing the smallest global RMSE. The analysis determines that Kd2 takes minimal values (4 × Kd1 in this model) (*25*). This indicates that the microscopic binding constants for the competitive binding site are of comparable magnitude to the primary site. Figure 7 shows the site specific fits to the global binding constants.

Some issues inherent in fitting 2D-NMR-monitored titration data to binding models are illustrated by the analysis for L121. For example, how should the chemical shift changes ($\Delta\delta$) in the two dimensions be summed? It is popular to use the Pythagorean formula, namely $\Delta\delta = (\Delta\delta_H^2 + \Delta\delta_N^2)^{1/2}$. Some workers advocate scaling the ^{15}N $\Delta\delta$ by $^1/_5$ before summing the two dimensions, to compensate for the inherently greater chemical shift dispersion of ^{15}N owing to the nucleus' more asymmetric shielding tensor. The motivation is to make changes in ^{15}N and ^{1}H similar when expressed in ppm. Figures 8A and C are two site, sequential fits to L121's data, when scaling of $\Delta\delta_N$ is used. Figures 8B and D show fits using data summed without scaling of $\Delta\delta_N$. Comparing Figures 8A and B shows that both forms of raw data are consistent with the same global Kds (the other two parameters in the model make compensatory changes). The global Kds are very roughly similar to the Kds obtained with careful local (nonglobal) fits (Figures 8C and D). The use of a global error function allows for

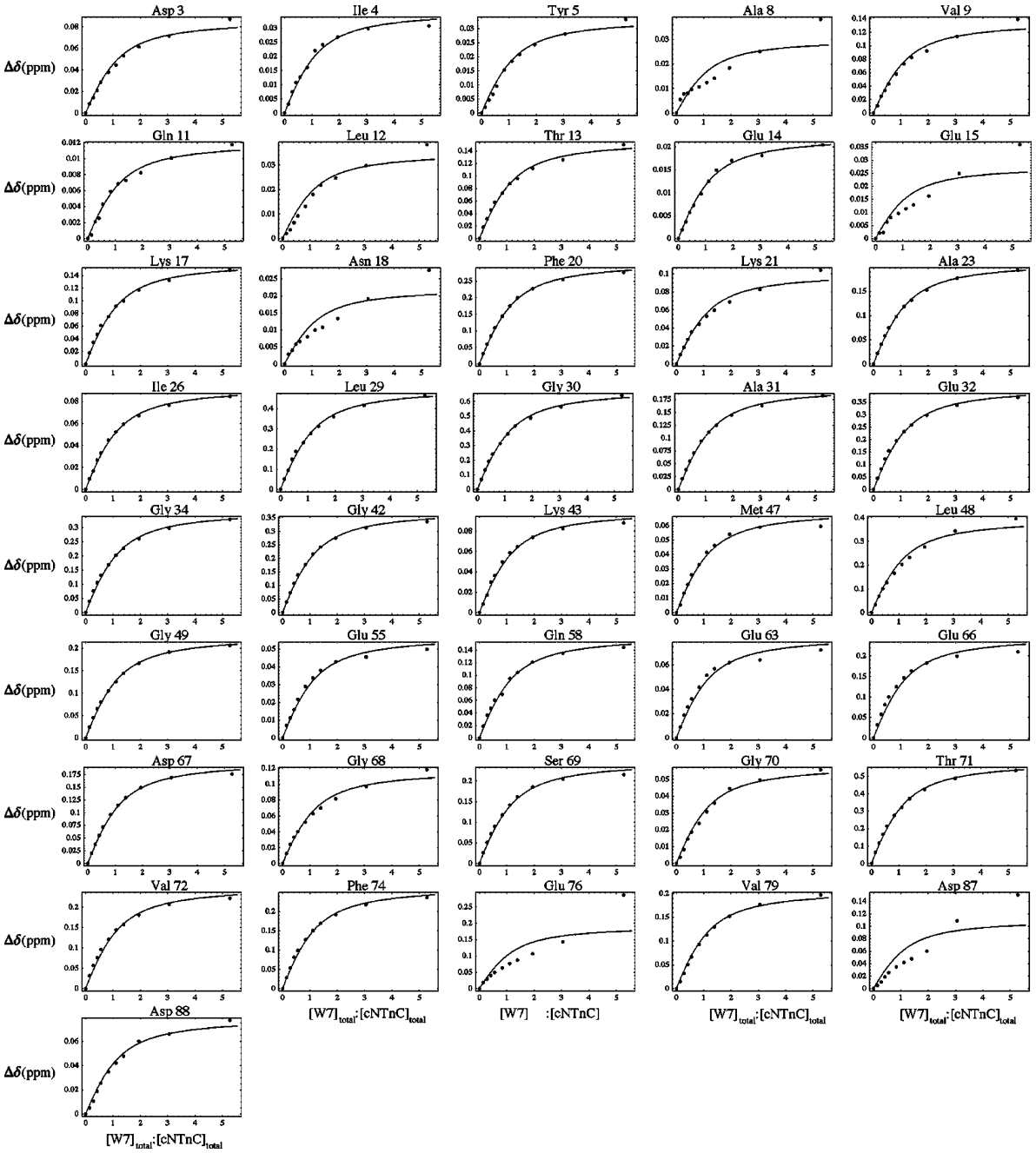

FIGURE 5: 41 of the 2D-{^{1}H,^{15}N}-HSQC cross-peaks, from the titration of cNTnC·Ca^{2+} with W7, fit to a single-site binding model (Kd = 0.22 mM). The raw titration data that is analyzed here is depicted in Figure 2. The global Kd was determined by repeating this fit while varying the Kd and minimizing a global error function (see Figure 4, left). The quality of the fit, considered on a residue-by-residue basis, is seen to be high.

maximum reconciliation of the 2D-NMR data with global binding constants.

DISCUSSION

Ligand binding to cTnC has received recent attention due to cTnC's pivotal regulatory role in cardiac muscle contraction. Drugs are sought to modulate cTnC's function within the scenarios of congestive heart failure and familial cardiac hypertrophy. Rational design of such pharmaceuticals is not, in both conceptual and practical senses, easy. cTnC is structurally homologous to skeletal TnC, CaM, and other members of the CaM-like superfamily. These structural similarities mostly stymie attempts to engineer specificity into a cTnC·ligand binding interaction. As well, cNTnC functions by altering its conformation in a ligand- and Ca^{2+}-dependent manner, so cardiotonic drug design requires acknowledgment of the interplay between protein structural dynamics and the canonical structure−activity concept. High-resolution NMR spectroscopy is well-suited to defining such relationships due to its ability to disclose extensive site-specific information from both stable and dynamic systems.

Figures 2 and 3 show many 2D-NMR cross-peaks shifting extensively as a function of $[W7]_{total}$. The distribution of {^{1}H,^{15}N}-chemical shift perturbations is shown in Figure 9, bottom. It is evident W7 binds to the domains of cTnC, perturbing their structures. This interpretation is favored over the alternative explanation of W7 promoting a wholly distinct fold, because a set of the cross-peaks are well-dispersed

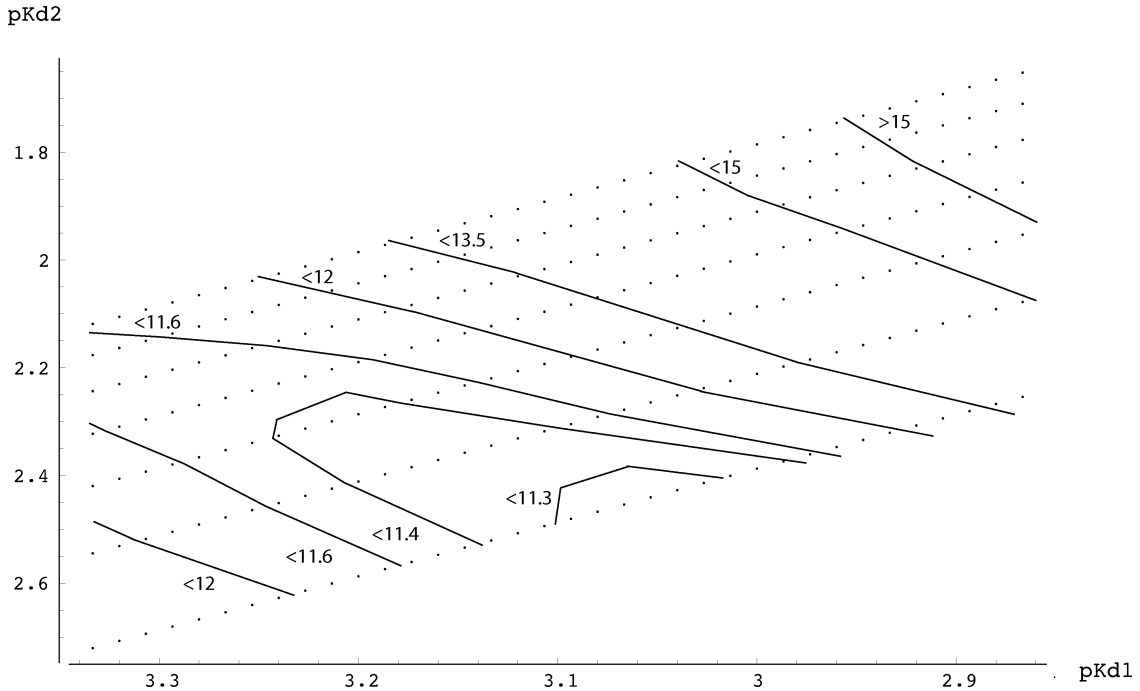

FIGURE 6: Determination of global Kds (Kd1 and Kd2) for a two-site, sequential binding model (*25*). The global RMSE is plotted as a function of pKd1 (horizontal axis) and pKd2 (vertical axis). The RMSE surface is sampled at 252 points. Contour lines show levels of constant RMSE. Labels are scaled by 1000 to improve readability. The global RMSE minimum occurs with Kd1 in the range $10^{-3.04}$–$10^{-3.07}$ (0.85−0.91 mM), and Kd2 = 4.001 × Kd1 (3.40−3.65 mM). The group of 6 points in the lowest contours have an RMSE <0.01112.

(reflecting a stable tertiary structure) and this dispersion is insensitive to W7 binding. The constructs used in this study lacked Cys residues (they are substituted with Ser). Previous studies have implied that C84 of cNTnC is required for the binding of levosimendan (*2*). Evidently, in the case of cNTnC·Ca^{2+}·W7, binding competency does not necessitate the presence of this residue, as was demonstrated for cNTnC·Ca^{2+}·bepridil. The presence of another ligand-coordinating residue could enhance the affinity of wild-type cNTnC for W7, however. Examination of Figures 5 and 7 shows that complete saturation of the binding sites was not accomplished, consistent with other binding studies of naphthalenesulfonamides (*12*, *14*, *15*). W7's limited solubility in water largely excludes the possibility of saturating the binding sites at the observed binding affinities and stoichiometries.

Addition of W7 shifts the NMR signals gradually over the titration. This indicates that W7 binding occurs in the exchanges in the NMR fast exchange limit, meaning that the exchange process is too rapid to allow separate observation of the free and bound signals. The exchange kinetics appear to be different between cCTnC·$2Ca^{2+}$·W7 and cNTnC·Ca^{2+}·W7: a handful of cNTnC's amide cross-peaks experience notable line broadening over the midpoints of the titration (Figure 2). The residues that are most severely broadened also shift substantially, consistent with the source of the broadening being the chemical exchange of W7. The distribution of broadened residues appears nonuniform because the extent of broadening is proportional to the change in chemical shift between the "bound" and "free" states. This suggests a slower exchange rate for cNTnC·Ca^{2+}·W7 compared with cCTnC·$2Ca^{2+}$·W7, consistent with cNTnC·Ca^{2+}·W7 being a more stable complex. A kinetic interpretation of the titration data is therefore consistent with the reported affinities.

In the titration of cCTnC·$2Ca^{2+}$, backbone and side chain signals both reflect binding heterogeneity (Figure 3). Many of the 2D-NMR peaks shift along a nonlinear path in the NMR spectra as W7 is added. Nonlinear trajectories of 2D-NMR signals throughout a titration series can indicate multiple binding events, with each binding event contributing a differing perturbation on the local magnetic environment. These observations reflect the impact of competition between differing binding sites or poses (possible if the population of a given pose is dependent on the concentration of W7). For cNTnC, the inherent native-state conformational exchange, indicated by line broadening and discrepancies between T2 and T1ρ measurements (*26*, *27*), may obscure the impact of binding heterogeneity on backbone resonances. That is to say, the chemical shift reported by {^{1}H,^{15}N}-coherences reflects averaging due to (at minimum) the exchange of ligand as well as the exchange of backbone conformations. The averaging of two dynamic processes may disallow observation of the two-state binding behavior at the backbone amide sites. The nonlinear 2D-NMR titration signals are demonstrated, however, by some {^{1}H,^{13}C}-HSQC signals of cNTnC (Figure 2). Mixed binding modes are oft-reported in this class of ligands (*15*, *28*). A review by Hidaka and Tanaka (*28*) summarized equilibrium binding studies of CaM·$4Ca^{2+}$·W7 (intact CaM) as consistent with both stronger (Kd = 11 μM, n = 3) and weaker (Kd = 200 μM, n = 9) binding events. Of course, other factors could account for the apparent two-state equilibrium implied by the titration data for cCTnC·$2Ca^{2+}$·W7. The solvation/desolvation of millimolar concentrations of W7 may significantly impact the observed chemical shift changes. The substantial changes in solvent composition over the titration are due to the presence of W7 (accompanied by the DMSO used to solvate it). Naphthalene is extremely hydrophobic, making W7 amphiphilic. This introduces the potential complication of

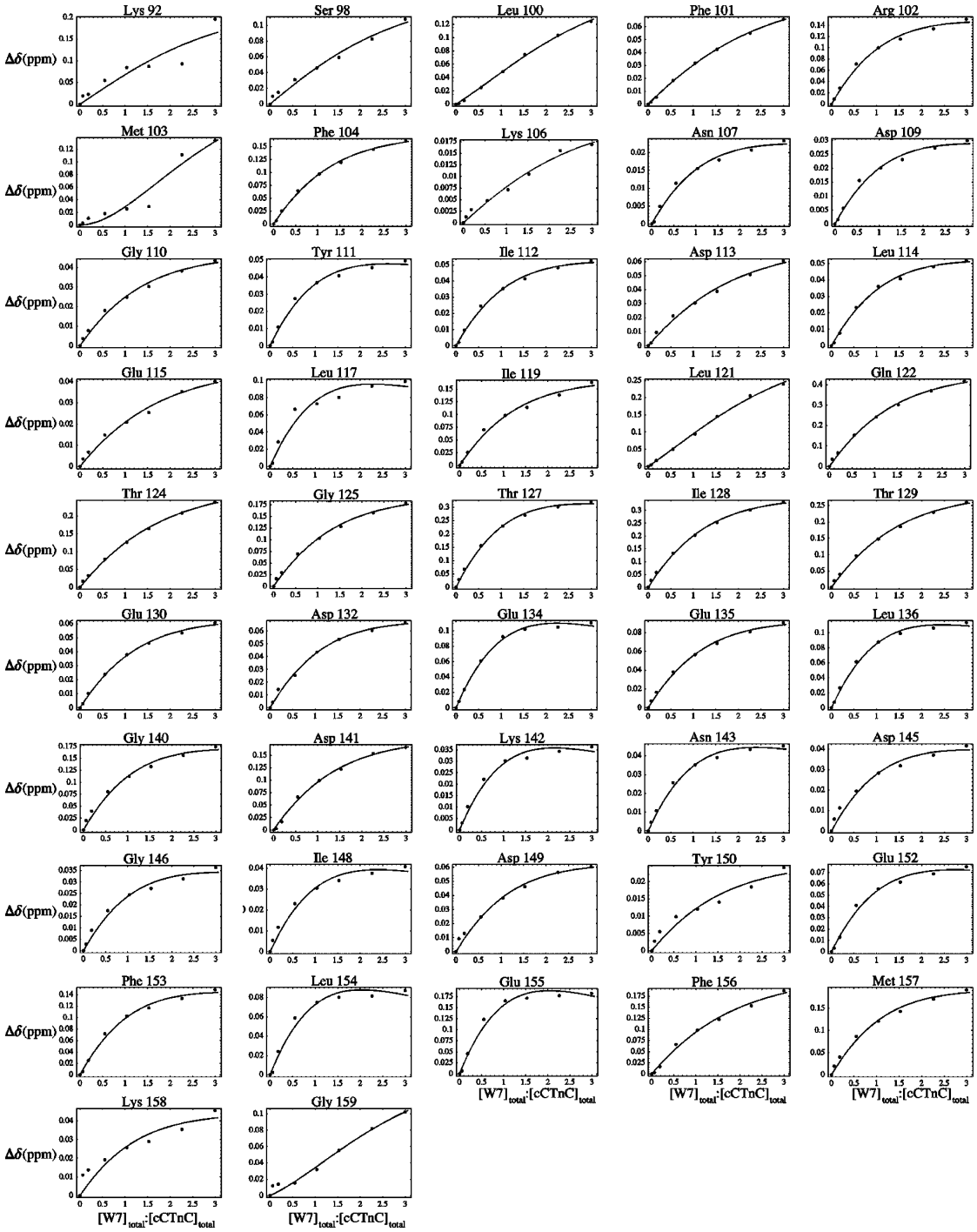

FIGURE 7: 47 of the 2D-{^{1}H,^{15}N}-HSQC cross-peaks from the titration of cCTnC·2Ca^{2+} with W7, fit to a two-site, sequential binding model (Kd1 = 0.88 mM; Kd2 = 3.5 mM). The raw titration data that is analyzed here is shown in Figure 3. The quality of the global fit is high, with few residues' fits having substantial outliers.

phase equilibria such as aggregation of W7. If aggregated W7 interacts with c(N/C)TnC, this could also account for the inflection points in the trajectories of 2D-NMR cross-peaks.

Examining the distribution of nonlinear trajectories in Figure 3, one can qualitatively localize the secondary binding events to the region bridging the two EF hands present in cCTnC. This region experiences the largest chemical shift perturbation over all portions of the titration (with or without scaling of ^{15}N). As previously discussed, interpreting curved HSQC trajectories due to a titration as two-site binding can present theoretical issues (*15*). For example, the HSQC resonance for L121 shifts predominantly in the ^{1}H dimension over the first increments of the titration (~0.5 ppm upfield), and nearly exclusively in the ^{15}N dimension (~0.75 ppm upfield) over the final increments (see Figure 3). These changes are difficult to reconcile with an interpretation of an enhanced local magnetic field at L121 due to orientations normal to W7's aromatic moiety. Such a rationale does not account for the apparent separation of the invoked local fields throughout the titration, as detected simultaneously by backbone amide nuclei. When expressed in ppm, the chemical shift should scale only with the perturbations to the local magnetic environment. The two nuclei of an amide group

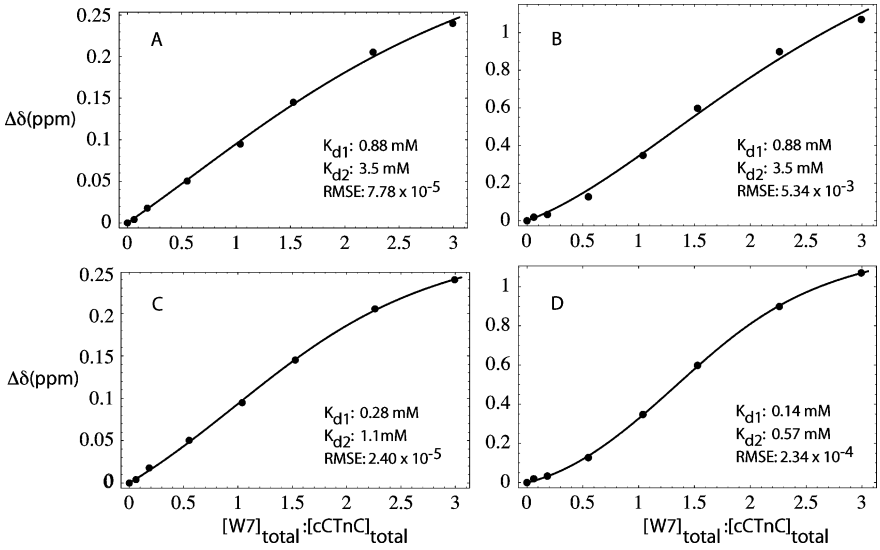

FIGURE 8: The {^{1}H,^{15}N}-HSQC NMR spectra collected over the titration of cCTnC·2Ca^{2+} with W7 (see Figure 3) can be analyzed in a number of ways. Here we show 4 different analyses of L121's data. (A,C) The raw data was scaled by 1/5 in the ^{15}N dimension before summing the ^{1}H and ^{15}N dimensions. (B,D) The same raw data is shown without the scaling of ^{15}N. Global fits (A, B), and local fits (C, D) are presented.

are separated by ~1 Å and are therefore, to a first approximation, in similar magnetic environments. ^{15}N, due to its large chemical shift anisotropy, is more sensitive to different conformations than ^{1}H, so the distribution of curved HSQC trajectories likely maps a [W7]-dependent conformational change rather than a direct ligand-mediated chemical shift perturbation (*15*).

Other observations further weaken a ligand-induced local-field interpretation of the chemical shift perturbations. The side chain amide group of Q58 presents two chemically nonequivalent protons shifting in opposite directions over the titration (Figure 2). This behavior is demonstrated by the same residues under activation by $cTnI_{147-163}$ (*24*). It is therefore likely that the behavior of Q58's NMR signals are only indirectly coupled to W7 binding. The side chain amide protons of Q50, however, shift in the same direction. Electrostatic fields can impinge upon protein atoms upon ligand binding. Such events perturb the chemical shift of the nuclei of polarizable atoms. A modeling study of the mechanism of Ca^{2+} sensitizers in cTnC (*9*) concluded that Q50 and D88 had long-range electrostatic interactions which impacted Ca^{2+} binding. This interaction was perturbed under binding of TFP, bepridil, or pimobendan. The present results support a functional role for Q50, which is clearly titratable (Figure 2). The chemical shift changes for the side chain of Q58, coupled simultaneously to other spectral changes indicative of the "opening" conformational transition of cNTnC·Ca^{2+}, show that W7 can directly modulate the functional conformational equilibria in cNTnC.

The Kds obtained in this study disagree (by more than an order of magnitude) with a previous report of the primary (strong) binding of W7 to TnC·4Ca^{2+} (*12*). It is difficult to reconcile this discrepancy because the previous study used intact chicken TnC, a distinct homologue, and different conditions. As well, the present study focuses on the domain-specific binding interactions, and attempts to characterize two binding sites for the cCTnC·2Ca^{2+}·W7 equilibrium. Two-site, sequential fits for cCTnC·2Ca^{2+}·W7 yield a Kd for the primary binding event of ~0.88 mM. It is important to note that the Kd for the secondary binding event, 3.5 mM, is the smallest possible Kd consistent with the model used, which requires Kd2 to be more than 4 times the value of Kd1. This indicates the secondary binding site to be similar in affinity to the primary one. The advantage of the model used is that the solution is analytic; the disadvantage is that because the model is stoichiometric and not explicitly site-specific, the binding constants obtained are difficult to interpret alongside the characteristically site-specific data generated by NMR. The stoichiometric picture presented here supports the theory that W7 is binding in multiple poses to cCTnC·2Ca^{2+}, alluding to the conclusions of Craven et al. in the study of CaM·4Ca^{2+}·J8 by NMR spectroscopy (*15*). The conclusion regarding J8 was obtained through an automated assignment of the intermolecular NOEs. Weak binding can reflect a larger external (mechanical/configurational) entropy for the ligand in the bound state (*29*) raising the issue of whether an atomic-resolution description of weak binding is possible without deconvolution of the ensemble-averaged observables.

Estimations of the stoichiometry of binding, when coupled with the spatial distribution of binding sites (Figure 9), directly imply the primary binding sites for W7 in cTnC (both domains) to be the functionally important hydrophobic pocket. This is a suitable location to allow W7 to disrupt interactions with cTnI (*30*) as proposed by Adhikari and Wang (*13*). Adhikari and Wang consider (and exclude) the interpretation that another protein, including myosin light chain kinase, is W7's target; this possibility not addressed by the present work. The affinity of $cTnI_{147-163}$ for cNTnC·Ca^{2+} is 0.154 ± 0.01 mM (*24*), similar to the affinity of W7 for cNTnC·Ca^{2+} determined in this study (0.22 mM). We expect that W7 binding to cTnC interferes with the binding of cTnI; as previously asserted, if most Met residues in cNTnC simultaneously interact with a ligand, this would likely disallow cTnI binding (*10*). The side chains of M45, M47, and M80 cannot simultaneously interact with a ligand while preserving the orientation of the B helix (see Figure 9). Rationalization of W7's affinity for cCTnC·2Ca^{2+} is more difficult given that the main site of regulation is cNTnC (*1*).

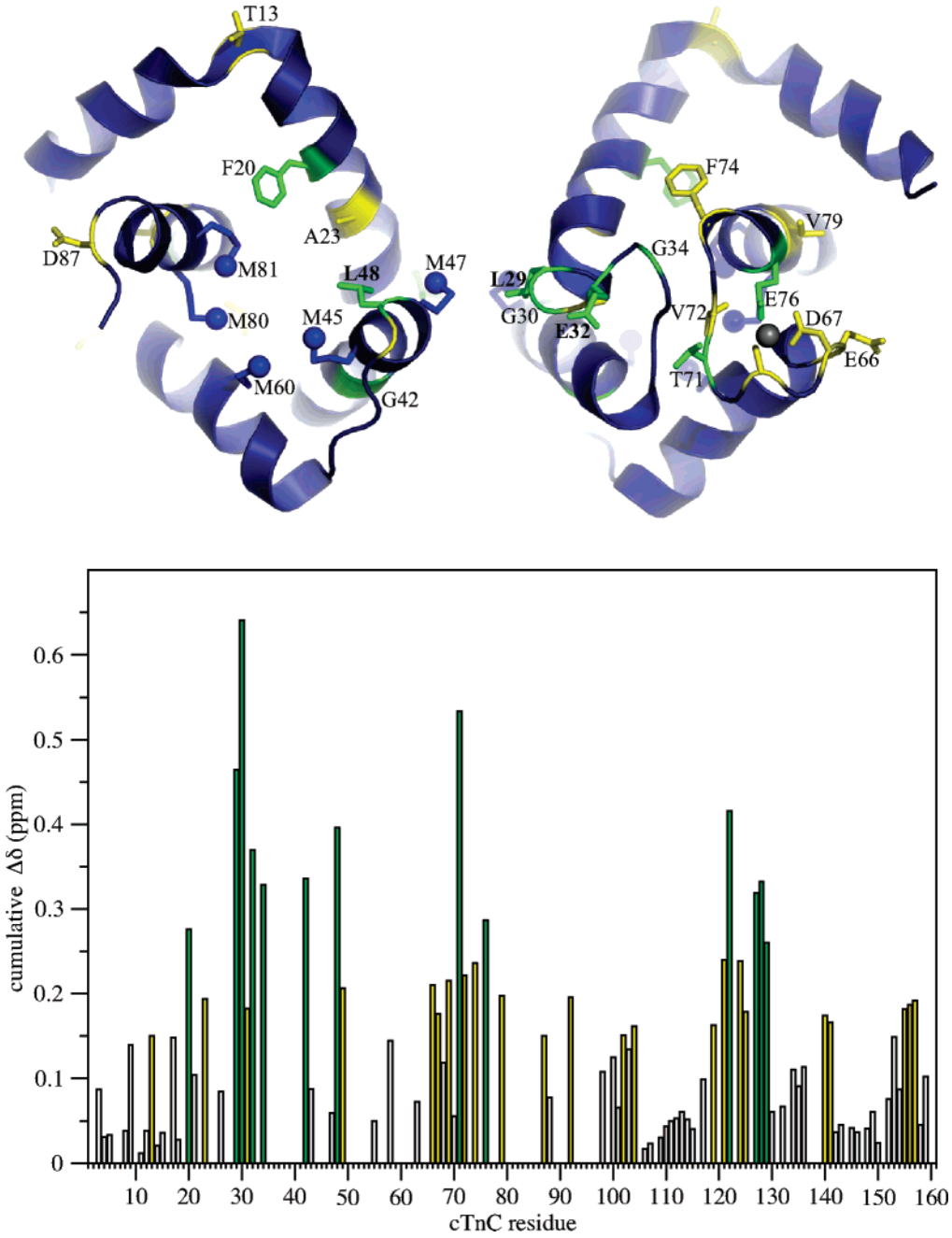

FIGURE 9: Sites in cNTnC with large {^{1}H,^{15}N}-chemical shift perturbations upon W7 binding. Bottom: Total $\Delta\delta$ vs cTnC residue number. Total changes > 0.25 ppm are colored green, changes > 0.15 ppm are colored yellow. Top: cNTnC·Ca^{2+} (PDB acession 1LXF, (*6*)) depicted in cartoon, with sites of large $\Delta\delta$ being colored to match the graph below. Top left: The Met side chains lining the hydrophobic pocket (see Figure 2) are shown in blue, with the Cϵ groups depicted as blue spheres. Top right: The Ca^{2+} binding sites of cNTnC. Ca^{2+} is shown as a gray sphere.

These observations prompt the further characterization of the binding of W7 to EF-hand-containing proteins, determination of high-resolution structures of cNTnC·Ca^{2+}·W7 and cCTnC·2Ca^{2+}·W7, and detailed dissection of the thermodynamic changes in protein and solvent due to W7 binding. The W7 binding site on cTnC also binds trifluoperazine (*16*), bepridil (*6*), EMD 57033 (*7*), Anapoe (*8*), and likely levosimendan (*31*, *32*). The extension of the current studies to the intact cTnC·3Ca^{2+}·W7 system should allow for more detailed descriptions of the biological significance of the structures presented here, as well as the family of cTnC·ligand complexes studied to date.

ACKNOWLEDGMENT

Pascal Mercier (Chenomx Inc.), Robert Boyko, and Olivier Julien provided invaluable assistance with software. Angela Thiessen and David C. Corson expressed and purified all protein samples. Jeffrey S. DeVries diligently maintained our NMR spectrometers.

SUPPORTING INFORMATION AVAILABLE

Input data (assigned NMRView peak lists) and the (Per1 and Mathematica) scripts used to obtain global Kds. This material is available free of charge via the Internet at http://pubs.acs.org.

REFERENCES

1. Sykes, B. D. (2003) Pulling the calcium trigger, *Nat. Struct. Biol. 10*, 588−589.
2. Sorsa, T., Pollesello, P., and Solaro, R. J. (2004) The contractile apparatus as a target for drugs against heart failure: interaction of levosimendan, a calcium sensitiser, with cardiac troponin c, *Mol. Cell. Biochem. 266*, 87−107.
3. Li, M. X., Wang, X., and Sykes, B. D. (2004) Structural based insights into the role of troponin in cardiac muscle pathophysiology, *J. Muscle Res. Cell Motil. 25*, 559−579.
4. Endoh, M. (2002) Mechanisms of action of novel cardiotonic agents, *J. Cardiovasc. Pharmacol. 40*, 323−338.
5. Levijoki, J., Pollesello, P., Kaivola, J., Tilgmann, C., Sorsa, T., Annila, A., Kilpelainen, I., and Haikala, H. (2000) Further evidence for the cardiac troponin C mediated calcium sensitization by levosimendan: structure-response and binding analysis with analogs of levosimendan, *J. Mol. Cell. Cardiol. 32*, 479−491.
6. Wang, X., Li, M. X., and Sykes, B. D. (2002) Structure of the regulatory N-domain of human cardiac troponin C in complex with human cardiac troponin I147−163 and bepridil, *J. Biol. Chem. 277*, 31124−31133.
7. Wang, X., Li, M. X., Spyracopoulos, L., Beier, N., Chandra, M., Solaro, R. J., and Sykes, B. D. (2001) Structure of the C-domain of human cardiac troponin C in complex with the Ca2+ sensitizing drug EMD 57033, *J. Biol. Chem. 276*, 25456−25466.
8. Vinogradova, M. V., Stone, D. B., Malanina, G. G., Karatzaferi, C., Cooke, R., Mendelson, R. A., and Fletterick, R. J. (2005) Ca2+-regulated structural changes in troponin, *Proc. Natl. Acad. Sci. U.S.A. 102*, 5038−5043.
9. Ovaska, M., and Taskinen, J. (1991) A model for human cardiac troponin C and for modulation of its Ca2+ affinity by drugs, *Proteins 11*, 79−94.
10. Kleerekoper, Q., Liu, W., Choi, D., and Putkey, J. A. (1998) Identification of binding sites for bepridil and trifluoperazine on cardiac troponin C, *J. Biol. Chem. 273*, 8153−8160.
11. Li, Y., Love, M. L., Putkey, J. A., and Cohen, C. (2000) Bepridil opens the regulatory N-terminal lobe of cardiac troponin C, *Proc. Natl. Acad. Sci. U.S.A. 97*, 5140−5145.
12. Hidaka, H., Yamaki, T., Naka, M., Tanaka, T., Hayashi, H., and Kobayashi, R. (1980) Calcium-regulated modulator protein interacting agents inhibit smooth muscle calcium-stimulated protein kinase and ATPase, *Mol. Pharmacol. 17*, 66−72.
13. Adhikari, B. B. and Wang, K. (2004) Interplay of troponin- and Myosin-based pathways of calcium activation in skeletal and cardiac muscle: the use of W7 as an inhibitor of thin filament activation, *Biophys. J. 86*, 359−370.
14. Osawa, M., Swindells, M. B., Tanikawa, J., Tanaka, T., Mase, T., Furuya, T., and Ikura, M. (1998) Solution structure of calmodulin-W-7 complex: the basis of diversity in molecular recognition, *J. Mol. Biol. 276*, 165−176.
15. Craven, C. J., Whitehead, B., Jones, S. K., Thulin, E., Blackburn, G. M., and Waltho, J. P. (1996) Complexes formed between calmodulin and the antagonists J-8 and TFP in solution, *Biochemistry 35*, 10287−10299.
16. Gariepy, J., and Hodges, R. S. (1983) Localization of a trifluoperazine binding site on troponin C, *Biochemistry 22*, 1586−1594.
17. Chandra, M., Dong, W. J., Pan, B. S., Cheung, H. C., and Solaro, R. J. (1997) Effects of protein kinase A phosphorylation on signaling between cardiac troponin I and the N-terminal domain of cardiac troponin C, *Biochemistry 36*, 13305−13311.
18. Li, M. X., Gagne, S. M., Tsuda, S., Kay, C. M., Smillie, L. B., and Sykes, B. D. (1995) Calcium binding to the regulatory N-domain of skeletal muscle troponin C occurs in a stepwise manner, *Biochemistry 34*, 8330−8340.
19. Hart, R. C., Bates, M. D., Cormier, M. J., Rosen, G. M., and Conn, P. M. (1983) Synthesis and characterization of calmodulin antagonistic drugs, in *Methods in Enzymology* Vol. 102, pp 195−204, Academic Press, Inc.: New York.
20. Delaglio, F., Grzesiek, S., Vuister, G. W., Zhu, G., Pfeifer, J., and Bax, A. (1995) NMRPipe: a multidimensional spectral processing system based on UNIX pipes, *J. Biomol. NMR 6*, 277−293.
21. Johnson, B. A. (2004) Using NMRView to visualize and analyze the NMR spectra of macromolecules, *Methods Mol. Biol. 278*, 313−352.
22. Boyko, R., and Sykes, B., http://www.bionmr.ualberta.ca/bds/software/xcrvfit/ accessed June 25, 2004.
23. Sia, S. K., Li, M. X., Spyracopoulos, L., Gagne, S. M., Liu, W., Putkey, J. A., and Sykes, B. D. (1997) Structure of cardiac muscle troponin C unexpectedly reveals a closed regulatory domain, *J. Biol. Chem. 272*, 18216−18221.
24. Li, M. X., Spyracopoulos, L., and Sykes, B. D. (1999) Binding of cardiac troponin-I147−163 induces a structural opening in human cardiac troponin-C, *Biochemistry 38*, 8289−8298.
25. Williams, T., Shelling, J., and Sykes, B. (1985) *NMR in the Life Sciences*, NATO ASI Series A: Life Sciences, pp 93−103, Plenum Publishing Co., New York.
26. Abbott, M. B., Gaponenko, V., Abusamhadneh, E., Finley, N., Li, G., Dvoretsky, A., Rance, M., Solaro, R. J., and Rosevear, P. R. (2000) Regulatory domain conformational exchange and linker region flexibility in cardiac troponin C bound to cardiac troponin I, *J. Biol. Chem. 275*, 20610−20617.
27. Paakkonen, K., Annila, A., Sorsa, T., Pollesello, P., Tilgmann, C., Kilpelainen, I., Karisola, P., Ulmanen, I., and Drakenberg, T. (1998) Solution structure and main chain dynamics of the regulatory domain (Residues 1-91) of human cardiac troponin C, *J. Biol. Chem. 273*, 15633−15638.
28. Hidaka, H. and Tanaka, T. (1983) Naphthalenesulfonamides as calmodulin antagonists, in *Methods in Enzymology* Vol. 102, pp 185−194, Academic Press, Inc.: New York.
29. Gilson, M., Given, J., Bush, B., and McCammon, J. (1997) The statistical-thermodynamic basis for computation of binding affinities: a critical review, *Biophys. J. 72*, 1047−1069.
30. Li, M. X., Saude, E. J., Wang, X., Pearlstone, J. R., Smillie, L. B., and Sykes, B. D. (2002) Kinetic studies of calcium and cardiac troponin I peptide binding to human cardiac troponin C using NMR spectroscopy, *Eur. Biophys. J. 31*, 245−256.
31. Pollesello, P., Ovaska, M., Kaivola, J., Tilgmann, C., Lundstrom, K., Kalkkinen, N., Ulmanen, I., Nissinen, E., and Taskinen, J. (1994) Binding of a new Ca2+ sensitizer, levosimendan, to recombinant human cardiac troponin C. A molecular modelling, fluorescence probe, and proton nuclear magnetic resonance study, *J. Biol. Chem. 269*, 28584−28590.
32. Sorsa, T., Pollesello, P., Permi, P., Drakenberg, T., and Kilpelainen, I. (2003) Interaction of levosimendan with cardiac troponin C in the presence of cardiac troponin I peptides, *J. Mol. Cell. Cardiol. 35*, 1055−1061.

BI051583Y